View metadata, citation and similar papers at core.ac.uk

brought to you by CORE

provided by Elsevier - Publisher Connector

Available online at www.sciencedirect.com

SCIENCE DIRECT

Biochimica et Biophysica Acta 1715 (2005) 122 – 131

BIOCHIMICA ET BIOPHYSICA ACTA BBA

http://www.elsevier.com/locate/bba

Divalent cations affect chain mobility and aggregate structure of lipopolysaccharide from *Salmonella minnesota* reflected in a decrease of its biological activity

Patrick Garidel[a], Michael Rappolt[b], Andra B. Schromm[c], Jörg Howe[c], Karl Lohner[d], Jörg Andrä[c], Michel H.J. Koch[e], Klaus Brandenburg[c,*]

[a]*Martin-Luther-Universität Halle/Wittenberg, Institut für Physikalische Chemie, Mühlpforte 1, D-06108 Halle, Germany*
[b]*Institut für Biophysik and Röntgenstrukturforschung, Österreichische Akademie der Wissenschaften, Synchrotron Triest, Strada Statale 14, I-34012 Basovizza (Trieste), Italy*
[c]*Forschungszentrum Borstel, Leibniz-Zentrum für Medizin und Biowissenschaften, Parkallee 10, D-23845 Borstel, Germany*
[d]*Institut für Biophysik and Röntgenstrukturforschung, Österreichische Akademie der Wissenschaften, Schmiedlstr. 6, A-8042 Graz, Austria*
[e]*European Molecular Biology Laboratory EMBL c/o Deutsches Elektronensynchrotron DESY, Notkestr. 52, D-22603 Hamburg, Germany*

Received 16 June 2005; received in revised form 28 July 2005; accepted 28 July 2005
Available online 18 August 2005

Abstract

The physicochemical properties and biological activities of rough mutant lipopolysaccharides Re (LPS Re) as preformed divalent cation (Mg^{2+}, Ca^{2+}, Ba^{2+}) salt form or as natural or triethylamine (Ten^{+})-salt form under the influence of externally added divalent cations were investigated using complementary methods: Differential scanning calorimetry (DSC) and Fourier-transform infrared spectroscopic (FT-IR) measurements for the $\beta \leftrightarrow \alpha$ gel to liquid crystalline phase behaviour of the acyl chains of LPS, synchrotron radiation X-ray diffraction studies for their aggregate structures, electron density calculations of the LPS bilayer systems, and LPS-induced cytokine (interleukin-6) production in human mononuclear cells. The divalent cation salt forms of LPS exhibit considerable changes in physicochemical parameters such as acyl chain mobility and aggregate structures as compared to the natural or monovalent cation salt forms. Concomitantly, the biological activity was much lower in particular for the Ca^{2+}- and Ba^{2+}-salt forms. This decrease in activity results mainly from the conversion of the unilamellar/cubic aggregate structure of LPS into a multilamellar one. The reduced activity also clearly correlates with the higher order – lower mobility – of the lipid A acyl chains. Both effects can be understood by an impediment of the interactions of LPS with binding proteins such as lipopolysaccharide-binding protein (LBP) and CD14 due to the action of the divalent cations.
© 2005 Elsevier B.V. All rights reserved.

Keywords: Cytokine; DSC; Electron density; Lipopolysaccharide; X-ray scattering

1. Introduction

Lipopolysaccharide (LPS) is the major lipid component from the outer leaflet of the outer membrane of Gram-negative bacteria. It is composed of a lipid moiety called lipid A and a covalently linked sugar part with a core oligosaccharide of different lengths (different rough mutants Re to Ra) and a polysaccharide part (O-antigen) determining the serotype specificity (smooth form LPS) [1]. The sugar part represents a barrier against invading drugs, while lipid A is mainly responsible for the variety of biological reactions, which LPS causes in mammals [2]. These reactions, which occur in a dose-dependent manner after release of LPS from the outer membrane, may be beneficial at low concentrations, but at high concentrations they may lead to pathophysiological effects including sepsis, septic shock, and multi-organ failure [3]. In all cases, the underlying cause of these effects is a release of cytokines such as tumor-necrosis-factor-α (TNFα) and

* Corresponding author. Fax: +49 4537 188632.
E-mail address: kbranden@fz-borstel.de (K. Brandenburg).

0005-2736/$ - see front matter © 2005 Elsevier B.V. All rights reserved.
doi:10.1016/j.bbamem.2005.07.013

interleukins by immunocompetent cells such as mononuclear cells (MNC).

Since LPS bears two negative charges in the lipid A part (1- and 4′-phosphates), and at least two further negative charges (carboxylates) in the adjacent 2-keto-3-deoxyoctonate (Kdo) moiety, the number and kind of counterions as well as the cation concentrations in buffers, in cell media, and of course in in vivo models are of high relevance. The influence of counterions on LPS structure was investigated by Snyder et al. [4], who found that divalent, but not monovalent cations led to LPS aggregation. Furthermore, it was found that the salt form influences the acyl chain and headgroup mobility of LPS [5] as well as the phase transition temperature of the acyl chains of the lipid A part of LPS and the state of order of the acyl chains at a given temperature [6], and that externally added divalent cations induce structural rearrangements of lipid A [7]. For a more detailed investigation of the influence of biologically relevant cations on LPS properties we have studied the influence of Mg^{2+} and Ca^{2+}, and partially also of Ba^{2+}, as counterion as well as externally added. It was found that the cations dramatically change biophysical parameters such as acyl chain order and aggregate structure, which might help to understand LPS action.

2. Materials and methods

2.1. Lipids and reagents

Lipopolysaccharide Re from the deep rough mutant *Salmonella minnesota* strain R595 was extracted by the phenol/chloroform/petrol ether method [8] from bacteria grown at 37 °C, purified, and lyophilized. This corresponds to the natural salt form of LPS. In this form, the main counterions are monovalent alkalines such as Na^+ and K^+ as well as some organic ions such as spermine and spermidine [1]. In low amounts also divalent counterions are found. Defined salt forms (triethylamine=Ten^+, Mg^{2+}, Ca^{2+}, Ba^{2+}) of LPS were produced by extensively dialysing (for at least 48 h) the natural salt form of LPS against the corresponding salt solutions (e.g., 1 mM $MgCl_2$, $CaCl_2$, $BaCl_2$), and subsequent lyophilisation.

2.2. Sample preparation

The lipid samples were usually prepared as aqueous dispersions (1 to 10 mM) for the phase transition measurements (FTIR, DSC), and down to 0.01 ng/ml for biological experiments. For X-ray diffraction, the concentration was 50 mM. The lipids were directly suspended in HEPES buffer, sonicated and temperature-cycled for several times between 5 and 70 °C and then stored at 4 °C for at least 12 h before measurement.

2.3. FTIR spectroscopy

Infrared spectra were recorded on a IFS-55 spectrometer (Bruker, Karlsruhe, Germany). The lipid samples were placed in a CaF_2 cuvette with a 12.5 μm teflon spacer, and the peak position of the symmetric stretching vibrational band ν_s (CH_2) of the methylene groups around 2850 cm^{-1} was recorded. Temperature-scans were performed automatically between 10 and 70 °C with a heating-rate of 0.6 °C/min. Every 3 °C, 50 interferograms were accumulated, apodized, Fourier transformed, and converted to absorbance spectra.

The infrared spectra were evaluated after base-line subtraction of neighbouring bands.

The order parameter S of the acyl chains ($S=1$ for perfectly aligned and=0 for isotropically distributed systems) was estimated from the peak position x_s of $\nu_s(CH_2)$ by a third order polynomial [9]

$$S = -941.8 + 0.7217x_s - 7.823 \times 10^{-5}x_s^2 - 2.068 \times 10^{-8}x_s^3.$$

2.4. Differential scanning calorimetry (DSC)

A stock solution of 1 mg/ml of LPS Re was dispersed in 10 mM phosphate buffer at pH 6.8. LPS aggregates were obtained by sonication as described previously [10,11]. Differential scanning calorimetry (DSC) measurements were performed with a MicroCal VP scanning calorimeter (MicroCal, Inc., Northhampton, MA, USA) at heating and cooling rates of 1 °C/min. Heating and cooling curves were measured between 10 and 95 °C. The accuracy of the temperature maximum of the heat capacity curve T_c is ±0.1 °C and for the phase transition enthalpy ±5%. Three consecutive heating and cooling scans were measured. For more details, see Blume and Garidel [12].

2.5. X-ray diffraction

The aggregate structures of the endotoxins were determined from X-ray diffraction patterns recorded on the double-focussing monochromator-mirror camera X33 of the European Molecular Biology Laboratory (EMBL) outstation at the Hamburg synchrotron radiation facility HASYLAB [13]. The patterns, obtained with exposure times of 2 min using a linear gas proportional detector with delay line readout [14] were evaluated according to previously described procedures [15]. These allow to assign the spacing ratios to defined three-dimensional aggregate structures.

2.6. Calculation of the electron density for multilamellar membrane stacks

The electron density profiles of the lipopolysaccharides in lamellar phases were derived from the small-angle X-ray diffractograms by standard procedures [16]. After correction of the experimental data for detector efficiency, and sub-

traction of the background scattering both from water and the sample cell, all Bragg peaks were fitted by Lorentzian distributions. Thereafter, a Lorentz correction was applied by multiplying each peak intensity (peak area) by the square of its corresponding wave vector s^2 [17]. The square root of the corrected peak intensity was finally used to determine the form factor F of each reflection. The electron density profile relative to the constant electron density of the solvent was calculated by the Fourier synthesis

$$\tilde{\rho}(z) = \sum_{h=1}^{h=4} F_h \cdot \cos\left(\frac{2\pi Hz}{d}\right),$$

where h is the order of reflection and d the lamellar spacing. For centrosymmetric crystals such as lamellar stacks of lipid bilayers, the electron density can be presented as a Fourier cosine series, where the unknown phases are either 0 (+) or π (−). The origin was set to the center of the bilayer by fixing the phase of the first order reflection to "−". All electron density profiles were reconstructed from 4 reflections, i.e., out of the possible $2^4=16$ combinations, the eight combinations centered at the middle of the terminal methyl dip were selected "−−−−, −−−+, −−+−, −−++, −+−−, −+−+, −++−, −+++". The most plausible phasing "−−+−" gives a profile that is quite similar to the hydrocarbon chain region of well-studied phospholipids [18] with a headgroup size of about 9 Å [19]. All other phase combinations lead to unplausible structural features, such as too large hydrocarbon core, missing methyl dip, or too small head group size. We note, that Snyder et al. [4] as well as Ding et al. [20] using the hydration variation method determined the same phase combination for Re LPS bilayer stacks in the gel-phase.

The decomposition of the lamellar d-spacing, d, into structural components such as bilayer thickness and fluid layer thickness is not trivial [21,22] and their errors lie typically in the range of a few tenths of Ångström. To keep the analysis as simple as possible, we discuss the bilayer thickness in terms of head to head group thickness, d_{HH} (cp. Fig. 3) and the water layer thickness in terms of $(d-d_{HH})$. The steric bilayer thickness d_B may be expressed as the sum of d_{HH} plus the head group size, d_H, which we define as the full width at half maximum of the maximum electron density distribution (cp. Fig. 3), i.e., $d_B=d_{HH}+d_H$. Correspondingly, the free fluid interface thickness d_W follows as $d_W=d-d_B$ [23] and the lipid chain length $d_C=d_{HH}/2-d_H/2$.

2.7. Stimulation of mononuclear cells

Peripheral blood mononuclear cells were isolated from whole heparinized (20 IU/ ml) blood of healthy donors by centrifugation on Ficoll density gradient. After washing three times with RPMI 1640 medium, the cells were resuspended in serum-free medium and equilibrated at 5×10^6 cells/ml. For stimulation, 200 μl per well of heparinized whole blood or mononuclear cells (5×10^6 cells/ml in RPMI medium) were placed in 96-well culture plates, and stimuli were added to the cultures at 20 μl per well. The cultures were incubated in 5% CO_2 for 24 h at 37 °C. Supernatants were collected and stored at −20 °C until the determination of cytokine levels. As cytokine interleukin-6 was determined in a bioassay using the murine cell line 7TD1 as described previously [24].

3. Results

3.1. Differential scanning calorimetry (DSC) of LPS Re

Three differential scanning calorimetric runs of a LPS Re sample, natural salt form, are presented in Fig. 1A yielding enthalpy changes $\Delta H_{Heating}=+39$ kJ/mol and $\Delta H_{Cooling}=-37$ kJ/mol with only slight variations in T_c and ΔH_c between the three scans. In further experiments also the influence of externally added Mg^{2+} (Fig. 1B) and the preformed Mg^{2+} salt form (not shown) was studied (see also Table 1). Fig. 1B illustrates that the phase transition temperature T_c (maximum of the heat capacity curve) increases in the presence of equimolar amounts of Mg^{2+} (from 32 to more than 36 °C), and that, in contrast to the natural salt form, the values of T_c as well as ΔH_c increase for the first three heating-scans. In further heating and cooling scans cycles, T_c and ΔH_c correspond, within the accuracy of the method, to the data as obtained for the third heating and cooling scan. An increase in T_c indicates that the gel phase is stabilized with respect to the liquid crystalline phase, and furthermore, that stronger interactions in the head group region of the lipid with the cation take place. An increase in ΔH_c is consistent with the formation of additional van der Waals contact areas between the hydrocarbon chains. This rearrangement seems to be favoured in the liquid crystalline phase.

Interestingly, during cooling scans the transition becomes very sharp indicating higher cooperativity, in contrast to the cooling scans for the natural salt form.

3.2. X-ray diffraction and electron density calculations of LPS Re

Synchrotron radiation X-ray diffraction was used to study the influence of divalent cations on the three-dimensional structure of LPS. The diffraction patterns of the Mg^{2+} salt and the natural salt form of LPS Re in the presence of externally added Mg^{2+} (Fig. 2) illustrate that the reflections are equally spaced characteristic for a multilamellar phase. Similar diffractograms were observed at temperatures up to 70 °C (not shown). This means that the mixed cubic/unilamellar aggregates that are observed at high water content (under near physiological conditions) [25] are converted into a multilamellar structure. The diffraction patterns look alike regardless of the temperature or chemical conditions, i.e., neither the peak shapes nor the peak widths change. This means that the lattice disorder of both phases is very similar and most probably the mechanical properties of

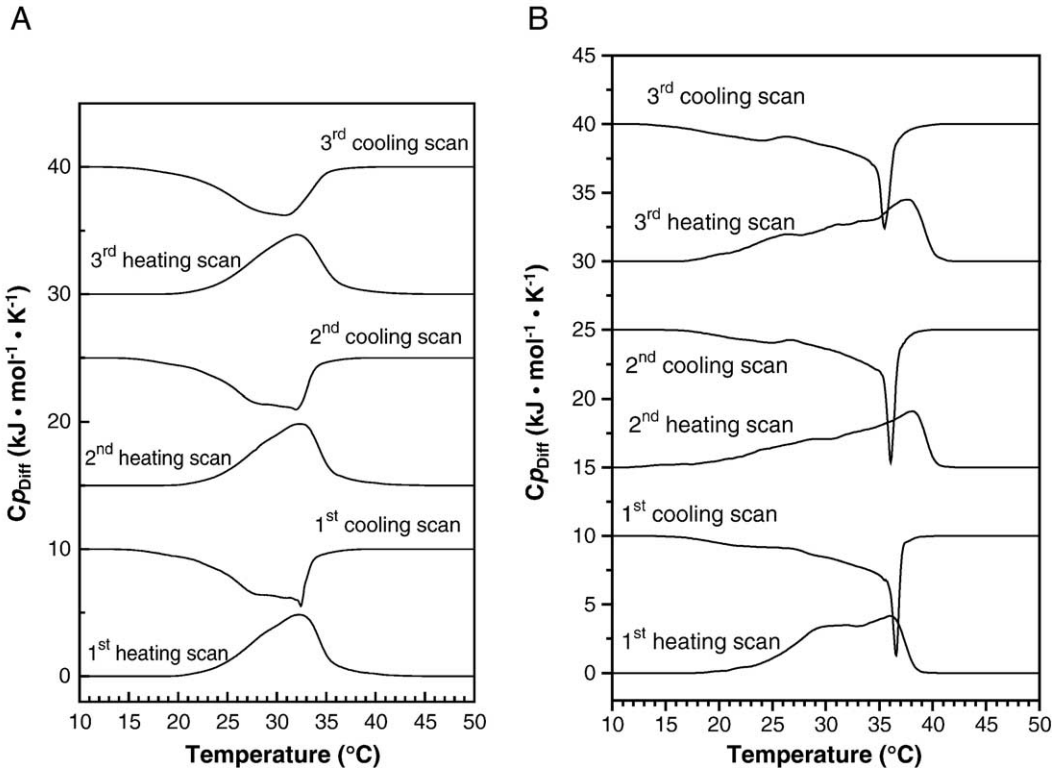

Fig. 1. Differential scanning calorimetric (DSC) scans of lipopolysaccharide LPS Re from *Salmonella minnesota* strain R595 in the natural salt form (A) and under the influence of externally added Mg^{2+} (equimolar, B). The LPS concentration was 1 mg/ml in buffer.

the bilayers do not alter much when the main transition is passed. Some samples showed additional traces of non-lamellar phases (see Fig. 2: arrows), but the lamellar phases were always predominant.

Table 1
Thermodynamic data of LPS Re (natural salt form), LPS Re Mg-salt, and in the presence of externally added Mg

Scan	ΔH_c (kJ mol^{-1})	T_c (°C)
LPS Re		
1st heating	+39	32.1
1st cooling	−37	32.4
2nd heating	+39	32.4
2nd cooling	−37	31.9
LPS Mg-salt		
1st heating	+43	36.2
1st cooling	−34	36.7
2nd heating	+46	37.0
2nd cooling	−34	36.7
3rd heating	+51	37.2
3rd cooling	−31	36.6
LPS Re + MgCl2 1:1 molar		
1st heating	+42	36.0
1st cooling	−31	36.6
2nd heating	+45	38.1
2nd cooling	−31	36.1
3rd heating	+49	37.7
3rd cooling	−34	35.5

For pure LPS Re, the data for the 3rd heating and cooling do not differ from those of the 2nd scans.

Similar results were obtained for the Mg^{2+} salt form of LPS (data not shown).

From the analysis of the peak diffraction intensities in Fig. 2, the electron density profile along the bilayer normal was determined and the decomposition of the lamellar periodicities d into its structural components was carried out (see Materials and methods). In Fig. 3, the different structural parameters of the bilayer system are explained. The example shows the natural LPS Re form in the presence

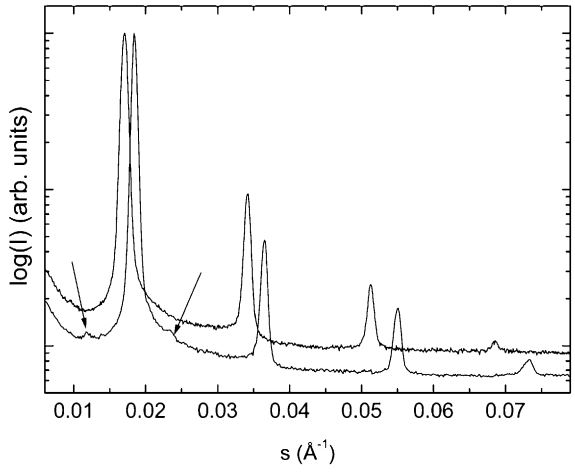

Fig. 2. Synchrotron radiation X-ray diffraction patterns of LPS Re from *Salmonella minnesota* strain R595 for the Mg^{2+} salt form (upper curve) and the natural salt form in the presence of externally added Mg^{2+} (lower curve) at 50 °C. The arrows indicate traces of non-lamellar structures.

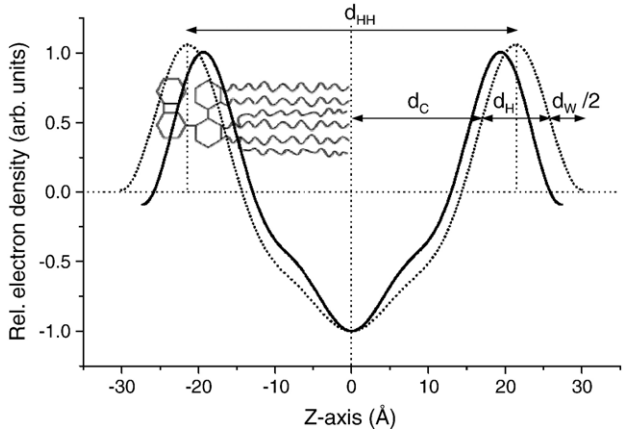

Fig. 3. Electron density profiles of the L_β (dotted) and L_α phase (solid) of the LPS Re from *Salmonella minnesota* strain R595 in the presence of externally added Mg^{2+}. At 20 °C the *d*-spacing is 60.2 Å and the head to head group distance d_{HH}=42.9 Å. The head group thickness d_H=8.8 Å and the hydrocarbon length d_C is 17 Å. In the fluid phase at 50 °C d= 54.7, d_{HH}=38.7, d_H=7.8, and d_C=15.4 Å.

of externally added Mg^{2+}. Comparing the L_β and L_α phase, we notice that in contrast to many other lipid systems the *d*-spacing does not change much. Within a temperature span of 30 °C the *d*-spacing decreases only by 5.5 Å. Thereby the main contribution is due to a reduction of the bilayer thickness, while the water layer thickness remains nearly constant. This can be another indication that bilayer fluctuations in the fluid lamellar phase are suppressed, however, it is also possible that attractive forces between the sugar headgroups of apposing bilayers are responsible for this as observed for cerebrosides [26].

The electron density distributions along the bilayer for the LPS Re Mg^{2+}-salt form (Fig. 4) yield similar results. However, in both lamellar phases – comparing the values at 20 and 50 °C – the head to head group thickness d_{HH} is about 2 Å larger and the water layer is about 1–2 Å increased, whereas the head group size of about 9 Å is invariant.

3.3. DSC of LPS Re Ca^{2+} salt form

The DSC data for LPS Re with external Ca^{2+} cations are shown in Fig. 5. The thermodynamic data together with those from the Ca^{2+} salt form of LPS are listed in Table 2. Comparison of these data with those in Table 1 demonstrates that Ca^{2+} induces a stronger increase in T_c than Mg^{2+} and a significantly reduced ΔH_c. The latter effect can be interpreted as reduced hydrocarbon chain interactions. As with the Mg^{2+} samples, the ΔH_c values increase between the first three scans, in particular for the Ca^{2+} salt form, indicating a rearrangement of the acyl chains.

3.4. X-ray diffraction and electron density of LPS Re Ca^{2+} salt form

As for all divalent salt forms of LPS Re also the small-angle X-ray diffraction data of the Ca^{2+} salt form exhibit the first four diffraction orders typical for multilamellar structures (data not shown). The evaluation of the electron density distribution (Fig. 6A, B) gives similar head-to-head group values d_{HH} as compared to the Mg^{2+} samples, but with a significantly lower periodicity, which essentially results from the much smaller water layer between neighbouring bilayers. This is an indication of dehydration effects in the polar head group regions as induced by the presence and tight binding of Ca^{2+}. This effect has been described previously for the interaction of alkaline earth cations with negatively charged phospholipids [27,28].

The Ba-salt form of LPS also gives diffraction patterns characteristic for a multilamellarization (data not shown). The evaluation of the electron density calculation is presented in Fig. 7, showing that the values of the water layer $d-d_{HH}$ are strikingly lower than those for the other cations.

In Fig. 8, an overview of the electron density profiles at 40 °C of all three salt-forms is given, and the structural parameters of the bilayer systems in the different salt forms in the liquid crystalline phase at 40 °C are summarized in Table 3.

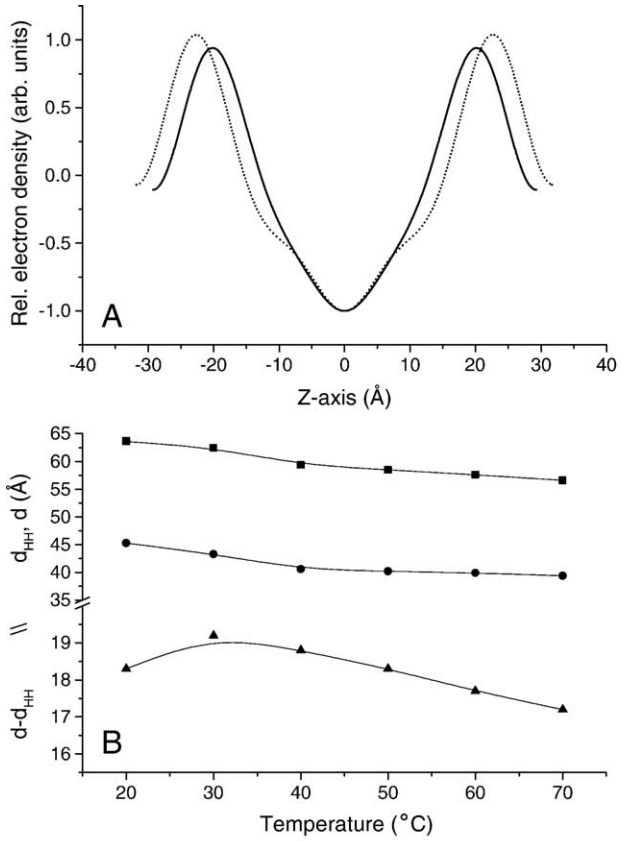

Fig. 4. Electron density distributions of the L_β (dotted) and L_α phase (solid) for LPS Re from *Salmonella minnesota* strain R595 for the Mg^{2+} salt form at 20 and 50 °C, respectively (A). Bilayer periodicities *d*, head to head group distances d_{HH}, and thicknesses of the water layer $d-d_{HH}$ are given from 20 to 70 °C (B).

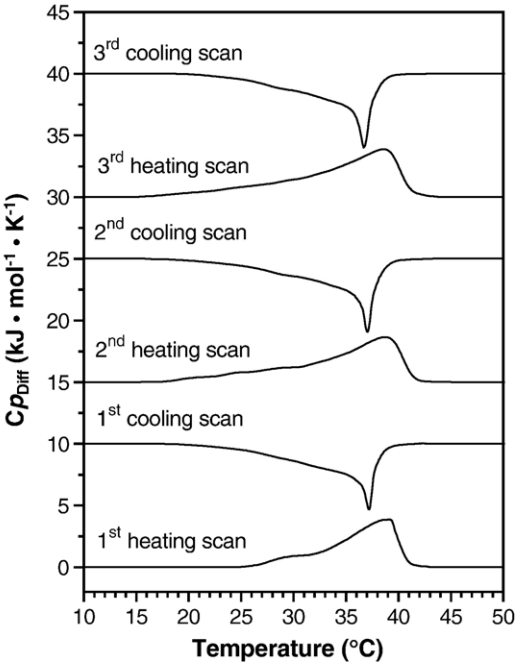

Fig. 5. DSC scans of LPS Re from *Salmonella minnesota* strain R595 in the presence of externally added Ca^{2+}. The LPS concentration was 1 mg/ml in buffer.

3.5. Phase transitions of LPS in various salt forms

The phase transition temperatures T_c of LPS Re in different salt forms was determined also with Fourier-transform infrared spectroscopy (FTIR) by analysing the symmetric stretching vibrational band, the peak position of which is located around 2849 to 2850 cm^{-1} in the gel and 2852 to 2853 cm^{-1} in the liquid crystalline phase, respectively [29]. The results shown in Fig. 9 are in agreement with the DSC scans (Figs. 1,5). Furthermore, as already found with the electron density profiles, the Ca^{2+} salt form of LPS Re differs from the Mg^{2+} salt form,

Table 2
Thermodynamic data of LPS Re Ca-salt and in the presence of externally added Ca

Scan	ΔH_c (kJ mol^{-1})	T_c (°C)
LPS Ca-salt		
1st heating	30	39.3
1st cooling	−23	37.5
2nd heating	36	39.0
2nd cooling	−21	37.2
3rd heating	49	38.9
3rd cooling	−22	37.1
LPS Re + $CaCl_2$ 1:1 molar		
1st heating	27	39.2
1st cooling	−26	37.2
2nd heating	35	38.7
2nd cooling	−28	37.1
3rd heating	38	38.5
3rd cooling	−27	36.7

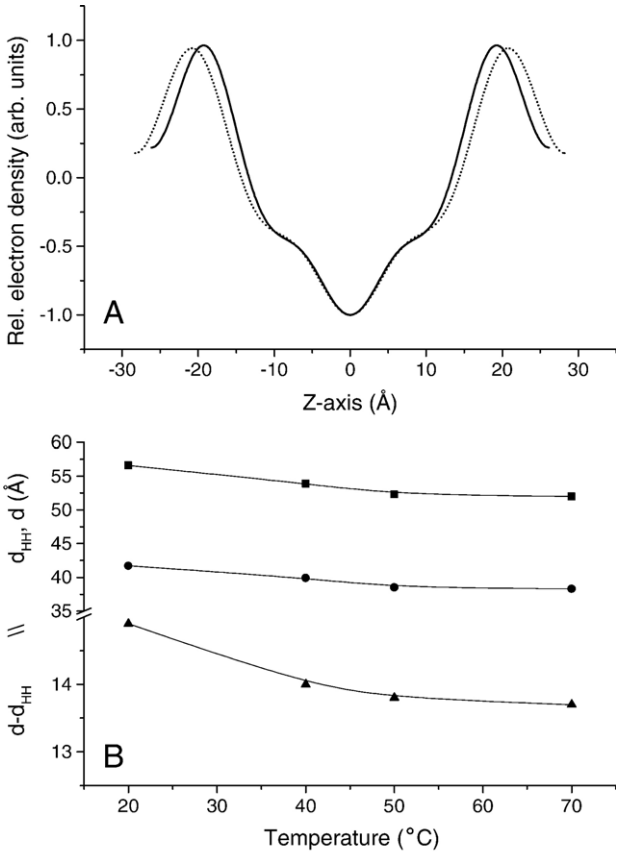

Fig. 6. Density maps of the L_β (dotted) and L_α phase (solid) for LPS Re from *Salmonella minnesota* strain R595 in the Ca^{2+} salt form at 90% content at 20 and 50 °C, respectively (A). Bilayer periodicities d, head to head group distances d_{HH}, and thicknesses of the water layer $d-d_{HH}$ are given from 20 to 70 °C (B).

the wavenumbers in both phases being significantly reduced, which is indicative of a reduced acyl chain mobility.

3.6. Biological activities of LPS in various salt forms

Finally, the biological activity of all salt forms of LPS Re was measured by determining its interleukin-6 inducing capacity in human mononuclear cells (Fig. 10). Clearly, the LPS in Ten^{+}- and natural salt form exhibit the strongest activity down to less than 100 pg/ml, while LPS in Mg^{2+} salt form is approximately 5 times less active. In contrast, LPS in the Ba^{2+} salt form and even more in its Ca^{2+} salt form is less active by orders of magnitude than the other salt forms.

3.7. Correlation of bioactivity with state of order of acyl chains

To compare the IL-6 inducing activity of LPS in the different salt forms, the amount of LPS, which is necessary to induce 10 ng/ml IL-6 (horizontal line in Fig. 10), is a useful measure. The results in Fig. 11 (top) unequivocally

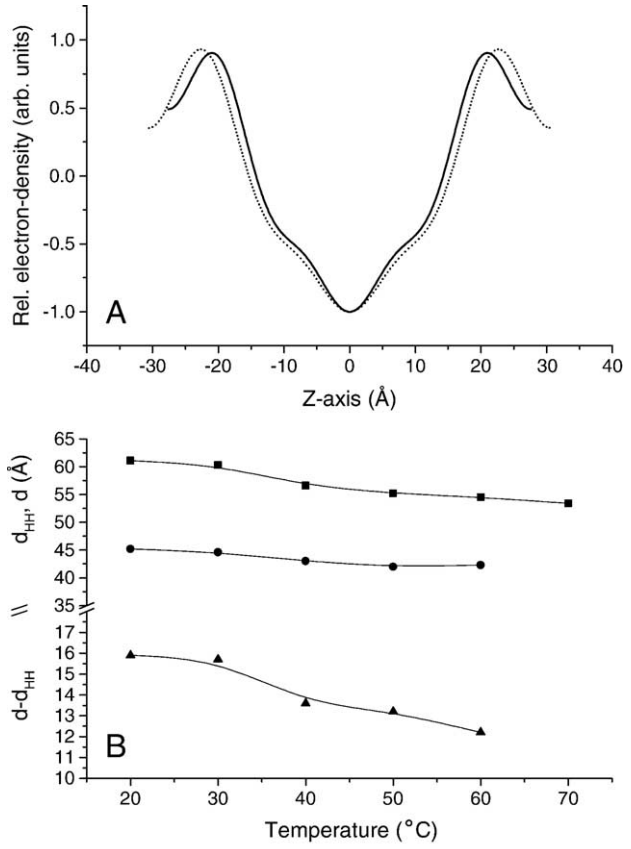

Fig. 7. Membrane density profiles of the L_β (dotted) and L_α phase (solid) for LPS Re from *Salmonella minnesota* strain R595 for the Ba^{2+} salt form at 90% buffer content at 20 and 50 °C, respectively (A). Bilayer periodicities d, head to head group distances d_{HH}, and thicknesses of the water layer $d-d_{HH}$ are given from 20 to 70 °C (B).

illustrate that the Ba^{2+}- and Ca^{2+}-salt forms correspond to the highest values (lowest activity). The values of the order parameter S of the acyl chains of the LPS, which was obtained from the wavenumber values at 37 °C in Fig. 9 according to the equation given in Materials and Methods, correlate with the biological activity. As can be clearly deduced from Fig. 11 (bottom), the LPS with lowest IL-6

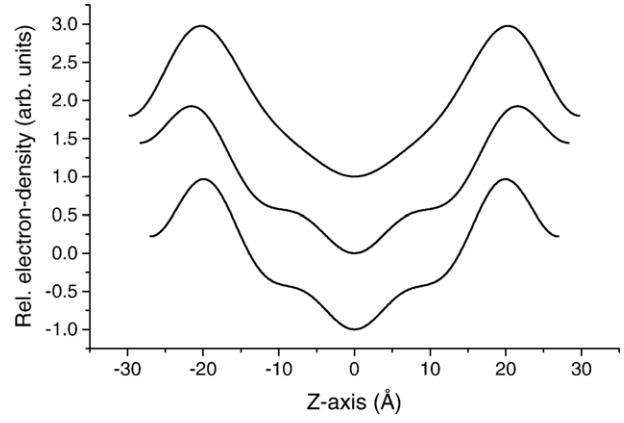

Fig. 8. Comparison of the bilayer profiles of LPS Re from *Salmonella minnesota* strain R595 for the Mg^{2+}, Ba^{2+} and Ca^{2+} salt form (from top to bottom).

Table 3
Structural parameters of the L_α-phase (at 40 °C) of LPS Re Mg^{2+}-salt, Ba^{2+}-salt, and Ca^{2+}-salt form, respectively

Structural parameters	LPS Re Mg^{2+} form	LPS Re Ba^{2+} form	LPS Re Ca^{2+} form
d-spacing [Å]	59.4	56.6	53.9
d_{HH} [Å]	40.6	43.0	39.9
$d-d_{HH}$ [Å]	18.8	13.6	14.0
d_H [Å]	9.3	8.2	7.5
d_C [Å]	15.7	17.4	16.2

The parameters were derived from the electron density profiles of Fig. 8. Beside the d-spacing, the head to head group distance d_{HH}, the head group thickness d_H and the hydrocarbon chain length d_C are given (cp. also Fig. 3).

inducing capacity have the highest S, i.e., lowest fluidity or mobility of their acyl chains and vice versa.

4. Discussion

In the present study, the influence of divalent cations, which are important constituents in all living systems, on structural parameters of preparations from deep rough mutant LPS Re, strain R595, were investigated. The physicochemical properties of the investigated systems are then correlated to their biological activity. The cations Mg^{2+}, Ca^{2+}, and Ba^{2+}, either as counterions or added as external agents, cause considerable changes of the structural polymorphism of LPS.

Whereas T_c as well as ΔH_c vary only negligibly for the natural salt form of LPS during the first three DSC scans (Fig. 1A), in the presence of external cations (Fig. 1B for Mg^{2+}) and for the Mg^{2+} and the Ca^{2+} (Fig. 5) salt forms considerable increases in T_c (see also Tables 1, 2) are observed. These are connected with an increase in the acyl chain order (increase in order parameter S) corresponding to a decrease of fluidity (Figs. 8 and 9). Interestingly, for LPS in Mg^{2+} forms (as counterion or as external agent), ΔH_c is higher than for the natural salt form in particular in the second and third heating-scan (Table 1), whereas the ΔH_c-values for LPS in the Ca^{2+} preparations (Table 2) are significantly lower. These are connected with an increase in the acyl chain order (increase in order parameter S) due to an increase in the trans configuration of the acyl chains. From the data as obtained for the first scan of the Ca^{2+} preparations, the ΔH_c-values are smaller compared to the data of the natural LPS form, although T_c of the Ca^{2+} systems are shifted up to 7 °C to higher temperature. With further temperature cycling, ΔH_c increases up to the third cycle, whereas T_c remains mainly unchanged. Such behaviour has been observed for calcium–phospholipid systems [27,28].

Three types of basic interactions of an external, charged agent with lipid membranes are described which lead to characteristic changes in the heat capacity curve: (a) electrostatic interactions often lead to an increase in the phase transition enthalpy with a concomitant increase in the

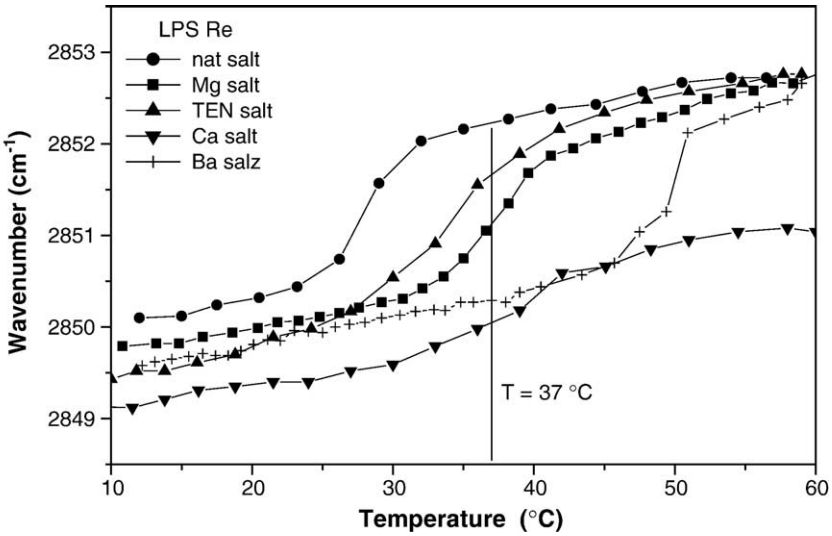

Fig. 9. Peak position of the symmetric stretching vibration of the methylene groups $\nu_s(CH_2)$ versus temperature for various salt forms of LPS Re from *Salmonella minnesota* strain R595. In the gel phase, the peak position is around 2849.5 to 2850 cm^{-1}, in the liquid crystalline phase around 2852 to 2852.5 cm^{-1}.

phase transition temperature; (b) electrostatic surface binding followed by partial penetration into the bilayer leading to more drastic changes in the phase transition enthalpy and temperature. The data indicate in most cases a decrease of the temperature and enthalpy, the latter being due to a decrease in chain and thus van der Waals interactions; (c) pre hydrophobic interactions of integral membrane proteins or hydrophobic agents lead to a more or less linear decrease of the phase transition enthalpy, which is correlated with the hydrophobic agent concentration. The half-width of the phase transition and thus the cooperativity is increased whereas only slight changes are detected for the maximum temperature of the heat capacity curve [30,31].

Based on these considerations, it can de deduced that type (a) interaction, i.e., pure electrostatic interactions is predominant. However, also dehydration effects induced by the presence of the divalent cations have to be considered.

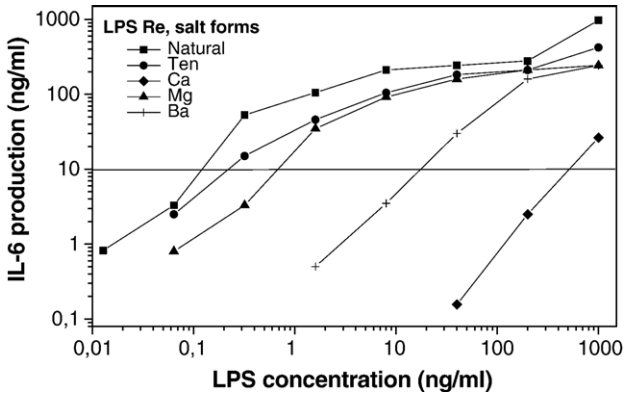

Fig. 10. Interleukin-6 production of human mononuclear cells induced by LPS Re from *Salmonella minnesota* strain R595 in different salt forms and the concentration range 10 pg/ml to 1 μg/ml.

Most importantly, the unilamellar/cubic inverted aggregate structures of LPS Re [24] are converted into multilamellar structures by divalent cations (Figs. 2, 4, 6, 7), independently of the kind of ion (Mg^{2+}, Ca^{2+}, Ba^{2+}). These data allow the calculation of the electron densities along the membrane normal, from which the geometry of the bilayer systems (Figs. 4, 6, 7) can be inferred. It has been shown that LPS or lipid A as multilamellar aggregate structure, either in pure form, such as for pentaacyl lipid A or LPS [32] or for hexaacyl lipid A or LPS in the presence of neutralizing proteins or peptides [33], are biologically inactive. Thus, the multilamellarization is a necessary condition for inactivation. In this way, the cytokine-inducing capacity of the LPS samples in the different salt forms (Fig. 10) becomes intelligible: there is an extreme decrease in the IL-6 production for the Ca^{2+}- and the Ba^{2+}-salt form of LPS, while the decrease for the Mg^{2+}-salt form is only moderate. A small remaining fraction (5–10%) of non-lamellar structure, which may not be detectable with X-ray diffraction (see, however, the arrows in Fig. 2), would suffice to explain the remaining IL-6 inducing activity. Furthermore, the water layer thickness in the Mg^{2+}-salt form is about 5 Å larger as compared to the other two forms (cp. Fig. 8 and Table 3), i.e., an enhanced free fluid volume might facilitate the diffusion of LPS-binding proteins such as lipopolysaccharide-binding protein (LBP).

The bilayer geometry for the different salts differs significantly. It is remarkable that the head group size clearly decreases from 9.3 Å for the Mg^{2+}-form (most active) down to 7.5 Å for the Ca^{2+}-salt form (least active) (Table 3). Even the fluidity of the chains in the Mg^{2+}-salt form appears to be highest of all, because the lipid chain length is the smallest. However, then the bilayer thickness of the Ca^{2+}-salt form should be greater than the Ba^{2+}-salt form, but this is not the case. Thus, considering also the activity and fluidity

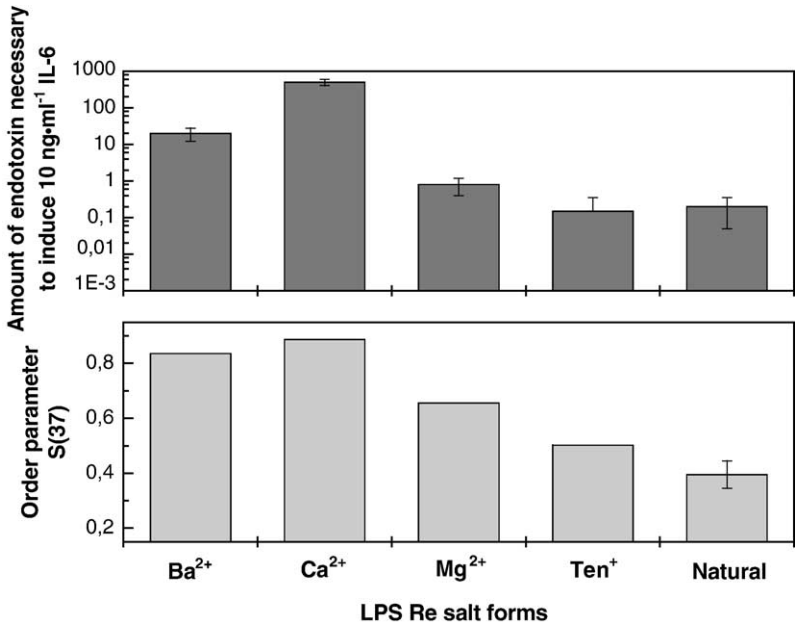

Fig. 11. Amount of LPS necessary to induce 10 ng/ml interleukin-6 (see Fig. 10, horizontal line) (top) and order parameter of the acyl chains (bottom) for lipopolysaccharide LPS Re from *Salmonella minnesota* strain R595 in different salt forms.

measurements (Figs. 9, 10), it is tempting to believe that a denser packing of the head group region is accompanied not only by an effective stiffening of the hydrocarbon chains, but also by an averaged tilt of the acyl chains. The latter would implicit an increase of the van der Waals hydrocarbon chains and thus an increase of the phase transition enthalpy (as is observed in the calorimetric experiments).

Few literature data are available on electron density calculations of LPS bilayers. Ding et al. [20] investigated LPS bilayers, partially also in the presence of cations, however, *a priori* as oriented multilamellar stacks. They found values of around 45 Å at 78 and 100% relative humidity, and around 42–43 Å in the presence of Ba^{2+}. The latter value is similar to what we have found here (Table 3), whereas no comparability is given for the former value, since LPS dispersions do not form multilamellar stacks.

Snyder et al. [4] investigated LPS-chemotypes from Re-, Rd-, Rc-, and Ra-mutants, also in the presence of divalent cations, and found for all LPS in the gel phase a value of 42 Å for the distances of the phosphate groups, which should correspond to the value of d_{HH}. This is nearly in accordance to our data for the Ca^{2+} salt form (Fig. 6), whereas for the Mg^{2+} (Fig. 4) and Ba^{2+}-salt form we find significantly higher values. It has to be taken into account, however, that the comparability may not be given since Snyder et al. prepared their multilayers at low rather than at high water content. A further determinant of bioactivity of LPS could be the acyl chain mobility. A large difference of cytokine-inducing activity between enterobacterial lipid A and LPS of two orders of magnitude was observed, and it was speculated that the high acyl chain order of lipid A (T_c= 45 °C) at 37 °C compared to LPS (T_c=30 to 35 °C) could account for this [34]. This is in agreement with the fact that for LPS and lipid A from *Coxiella burnetii*, which have the same acyl chain mobility at 37 °C, no difference in bioactivity (although it is reduced as compared to enterobacterial LPS) could be detected [35]. Thus, the acyl chain mobility is *a priori* not a determinant of endotoxin bioactivity, but may modulate it significantly. In this way, the high order parameter S of the arrangement of the acyl chains for the divalent cation salt form of LPS (Fig. 11) may contribute to their reduced cytokine-inducing activity. Moreover, an eleven amino acid fragment of human lactoferrin (LF11) and its N-acyl derivative also converted the unilamellar/cubic aggregate structure into multilayer ones, but in contrast to divalent cations, a disordering effect on the acyl chains (higher mobility) in the gel phase was observed in the presence of N-acyl-LF11 [36].

Acknowledgements

The authors are indebted to G. von Busse for assistance in IR and B. Fölting in DSC measurements. This study has been carried out with the financial support from the Deutsche Forschungsgemeinschaft (SFB367, project B8) and the Commission of the European Communities under the specific RTD program ‘Quality of Life and management of Living Resources’, QLK2-CT-2003-01001, ‘Antimicrobial endotoxin neutralizing peptides to combat infectious diseases’.

References

[1] E.Th. Rietschel, T. Kirikae, F.U. Schade, U. Mamat, G. Schmidt, H. Loppnow, A.J. Ulmer, U. Zähringer, U. Seydel, F. Di Padova, M.

Schreier, H. Brade, Bacterial endotoxin: molecular relationships of structure to activity and function, FASEB J. 8 (1994) 217–225.
[2] U. Zähringer, B. Lindner, E.T. Rietschel, Chemical structure of lipid A. Recent advances in structural analysis of a biologically active molecules, in: H. Brade, S.M. Opal, S.N. Vogel, D.C. Morrison (Eds.), Endotoxin in Health and Disease, 1999, pp. 93–114 (New York).
[3] U. Seydel, A.J. Ulmer, S. Uhlig, E.Th. Rietschel, Lipopolysaccharide, in: G. Zimmer (Ed.), Membrane Structure in Disease and Drug Therapy, Marcel Dekker, New York, Basel, 2000, pp. 217–252.
[4] S. Snyder, D. Kim, T.J. McIntosh, Lipopolysaccharide bilayer structure: effect of chemotype, core mutations, divalent cations, and temperature, Biochemistry 38 (1999) 10758–10767.
[5] R.T. Coughlin, A. Haug, E.J. McGroarty, Physical properties of defined lipopolysaccharide salts, Biochemistry 22 (1983) 2007–2013.
[6] K. Brandenburg, U. Seydel, Investigation into the fluidity of lipopolysaccharide and free lipid A membrane systems by Fourier-transform infrared spectroscopy and differential scanning calorimetry, Eur. J. Biochem. 191 (1990) 229–236.
[7] K. Brandenburg, M.H.J. Koch, U. Seydel, Phase diagram of lipid A from *Salmonella minnesota* and *Escherichia coli* rough mutant lipopolysaccharide, J. Struct. Biol. 105 (1990) 11–21.
[8] C. Galanos, O. Lüderitz, O. Westphal, A new method for the extraction of R lipopolysaccharides, Eur. J. Biochem. 9 (1969) 245–249.
[9] K. Brandenburg, H. Mayer, M.H.J. Koch, J. Weckesser, E.Th. Rietschel, U. Seydel, Influence of the supramolecular structure of free lipid A on its biological activity, Eur. J. Biochem. 218 (1993) 555–563.
[10] G. Jürgens, M. Müller, P. Garidel, M.H.J. Koch, H. Nakakubo, A. Blume, K. Brandenburg, Investigation into the interaction of recombinant human serum albumin with Re-lipopolysaccharide and lipid A, J. Endotoxin Res. 8 (2002) 115–126.
[11] K. Brandenburg, G. Jürgens, J. Andrä, B. Lindner, M.H.J. Koch, A. Blume, P. Garidel, Biophysical characterization of the interaction of high-density lipoprotein (HDL) with endotoxins, Eur. J. Biochem. 269 (2002) 5972–5981.
[12] A. Blume, P. Garidel, Lipid model membranes and biomembranes, in: R.B. Kemp (Ed.), From Macromolecules to Man, Elsevier, Amsterdam, 1999, pp. 109–173.
[13] M.H.J. Koch, J. Bordas, X-ray diffraction and scattering on disordered systems using synchrotron radiation, Nucl. Instrum. Methods 208 (1983) 461–469.
[14] A. Gabriel, Position-sensitive X-ray detector, Rev. Sci. Instrum. 48 (1977) 1303–1305.
[15] K. Brandenburg, W. Richter, M.H.J. Koch, H.W. Meyer, U. Seydel, Characterization of the nonlamellar cubic and H_{II} structures of lipid A from *Salmonella enterica* serovar Minnesota by X-ray diffraction and freeze-fracture electron microscopy, Chem. Phys. Lipids 91 (1998) 53–69.
[16] M. Rappolt, A. Hickel, F. Bringezu, K. Lohner, Mechanism of the lamellar/inverse hexagonal phase transition examined by high resolution X-ray diffraction, Biophys. J. 84 (2003) 3111–3122.
[17] C.R. Worthington, R.S. Khare, Structure determination of lipid bilayers, Biophys. J. 23 (1978) 407–425.
[18] P.E. Harper, D.A. Mannock, R.N. Lewis, R.N. McElhaney, S.M. Gruner, X-ray diffraction structures of some phosphatidylethanolamine lamellar and inverted hexagonal phases, Biophys. J. 81 (2001) 2693–2706.
[19] M. Rappolt, P. Laggner, G. Pabst, Structure and elasticity of phospholipid bilayers in the Lα phase: a comparison of phosphatidylcholine and phosphatidylethanolamine membranes, in: S.G. Pandalai (Ed.), Recent Res. Devel. Biophys. vol. 3, Part II, Transworld Research Network, Trivandrum, pp. 363–392.
[20] L. Ding, L. Yang, T.M. Weiss, A.J. Waring, R.I. Lehrer, H.W. Huang, Interaction of antimicrobial peptides with lipopolysaccharides, Biochemistry 42 (2003) 12251–12259.
[21] J.F. Nagle, S. Tristram-Nagle, Structure of lipid bilayers, Biochim. Biophys. Acta 1469 (2000) 159–195.
[22] G. Pabst, M. Rappolt, H. Amenitsch, P. Laggner, Structural information from multilamellar liposomes at full hydration: full q-range fitting with high-quality X-ray data, Phys. Rev., E 62 (2005) 4000–4009.
[23] T.J. McIntosh, S.A. Simon, Hydration force and bilayer deformation: a reevaluation, Biochemistry 25 (1986) 4058–4066.
[24] A.B. Schromm, K. Brandenburg, H. Loppnow, U. Zähringer, E.Th. Rietschel, S.F. Carroll, M.H.J. Koch, S. Kusumoto, U. Seydel, The charge of endotoxin molecules influences their conformation and interleukin-6 inducing capacity, J. Immunol. 161 (1998) 5464–5471.
[25] K. Brandenburg, M.H.J. Koch, U. Seydel, Phase diagram of deep rough mutant lipopolysaccharide from *Salmonella minnesota* R595, J. Struct. Biol. 108 (1992) 93–106.
[26] K. Kulkarni, D.S. Snyder, T.J. McIntosh, Adhesion between cerebroside bilayers, Biochemistry 38 (1999) 15264–15271.
[27] P. Garidel, A. Blume, Interaction of alkaline earth cations with the negatively charged phospholipid 1,2-dimyristoyl-*sn*-glycero-3-phosphoglycerol, Biophys. Biochem. Acta 1466 (2000) 245–259.
[28] P. Garidel, G. Förster, W. Richter, N. Kunst, G. Rapp, A. Blume, 1,2-Dimyristoyl-*sn*-glycero-3-phosphoglycerol (DMPG) divalent cation complexes: an X-ray scattering and freeze fracture electron microscopy study, Phys. Chem. Chem. Phys. 2 (2000) 4537–4544.
[29] H.H. Mantsch, R.N. McElhaney, Phospholipid phase transitions in model and biological membranes as studied by infrared spectroscopy, Chem. Phys. Lipids 57 (1991) 213–226.
[30] A. Blume, Biological calorimetry: membranes, Thermochim. Acta 193 (2005) 229–347.
[31] D. Papahadjopoulos, Effects of proteins on thermotropic phase transitions of phospholipid membranes, Biochim. Biophys. Acta 401 (1975) 317–335.
[32] A.B. Schromm, K. Brandenburg, H. Loppnow, A.P. Moran, M.H.J. Koch, E.Th. Rietschel, U. Seydel, Biological activities of lipopolysaccharides are determined by the shape of their lipid A portion, Eur. J. Biochem. 267 (2000) 2008–2013.
[33] K. Brandenburg, G. Jürgens, M. Müller, S. Fukuoka, M.H.J. Koch, Biophysical characterization of lipopolysaccharide and lipid A inactivation by lactoferrin, Biol. Chem. 382 (2001) 1215–1225.
[34] U. Seydel, H. Labischinski, M. Kastowsky, K. Brandenburg, Phase behaviour, supramolecular structure, and molecular conformation of lipopolysaccharide, Immunobiology 187 (1993) 191–211.
[35] R. Toman, P. Garidel, J. Andrä, K. Slaba, A. Hussein, M.H.J. Koch, K. Brandenburg, Physicochemical characterization of the endotoxins from *Coxiella burnetii* strain Priscilla in relation to their bioactivities, BMC Biochem. 5 (2004) 1.
[36] J. Andrä, K. Lohner, S.E. Blondelle, R. Jerala, I. Moriyon, M.H. Koch, P. Garidel, K. Brandenburg, Enhancement of endotoxin neutralization by coupling of a C12-alkyl chain to a lactoferricin-derived peptide, Biochem. J. 385 (2005) 135–143.